Case History of Risk Evaluation of Earth-Fill Dams Due to Heavy Rain

Toshifumi Shibata, *Associate Professor, Okayama University, Okayama, Japan; email: tshibata@cc.okayama-u.ac.jp*
Shin-ichi Nishimura, *Professor, Okayama University, Okayama, Japan; email: theg1786@cc.okayama-u.ac.jp*
Tsubasa Tateishi, *Graduate Student, Okayama University, Okayama, Japan; email: plb65pco@s.okayama-u.ac.jp*
Shuichi Kuroda, *Eight-Japan Engineering Consultants Inc., Okayama, Japan; email: kuroda-shu@ej-hds.co.jp*
Tomoo Kato, *Eight-Japan Engineering Consultants Inc., Okayama, Japan; email: katou-to@ej-hds.co.jp*
Kentaro Kuribayashi, *Eight-Japan Engineering Consultants Inc., Okayama, Japan; email: kuribayashi-ke@ej-hds.co.jp*
Namihiko Tanaya, *Eight-Japan Engineering Consultants Inc., Okayama, Japan; email: tanaya-na@ej-hds.co.jp*

ABSTRACT: *The present paper describes an assessment method for risks brought on by heavy rain in order to determine the priority of countermeasures for small earth-fill dams. To evaluate the failure risks of an earth-fill dam, defined as the product of failure probability and damage costs, an unsaturated seepage flow analysis is carried out based on the measured rainfall conditions. The damage costs are calculated using the correlation between the results of a flood analysis after breaching and land use and asset data. Subsequently, an evaluation to prioritize the countermeasures is conducted based on the failure risks. The larger of the two comparative failure probabilities—namely, the probability of overflow and the probability of slip failure—will showcase the dominant factor in the failure of small earth-fill dams, and the failure risk evaluation will determine the priority of the countermeasures for repairing and/or reinforcing decrepit earth-fill dams.*

KEYWORDS: earth-fill dam, risk evaluation, prioritization, heavy rain

SITE LOCATION: **Geo-Database**

INTRODUCTION

There are approximately 170,000 earth-fill dams in Japan. The dams are located densely in the Chugoku Region of Japan along the Seto Inland Sea. Approximately 20,000 of these earth-fill dams, used for irrigation and water supply, are found in Hiroshima Prefecture. Since many of the dams were constructed hundreds of years ago, several of them have been damaged over the years by heavy rain and earthquakes, causing them to become decrepit. Most of the damage to the small earth-fill dams was caused by heavy rain, such as that brought about by typhoons or *baiu* rainfall, frequently leading to downstream floods that have had a great impact on the hydraulic structures used for irrigation and drainage.

The number of heavy rain events has been increasing recently because of climate change. The number of floods, and hence, the damage due to flooding, have also increased (United Nations Office for Disaster Risk Reduction 2018). Considerable attention has been drawn to the various problems of climate change and its broader implications related to economic development, and many studies modeling river flood hazards have been conducted. Kazama et al. (2009) dealt with such economic damage as the destruction of economic assets and infrastructure in Japan. Their study adopted the numerical results of 2D non-uniform flow models using land use grid data, while the relationship between the damage rate and the inundation depth was obtained from the flood control economy investigation manual published by the Ministry of Land, Infrastructure, Transport, and Tourism (2005).

Tanoue et al. (2019) focused on estimating the economic losses due to the 2011 Thailand flood, over a long inundation period, using a computable general equilibrium model. Mirza (2002) reported the implications of flooding in Bangladesh using hydrological and damage data. Naess et al. (2005) reported the role that institutions play in climate adaptation in Norway, and Hirabayashi et al. (2013), Alfieri et al. (2018), and Winsemius et al. (2015) presented the global river flood risks. Jonkman and Vrijling (2008) showed an overview of the research on loss of life due to floods. Thus far, however, only a few attempts have been made to examine the flood risks of small earth-fill dams, even though numerous dams of this type exist in Japan and have frequently experienced serious damage. For example, the heavy rain event of July 2018 caused the breaching of 32 small earth-fill dams, principally in Hiroshima Prefecture, resulting in massive damage to housing and farming fields in the downstream area.

After the heavy rain event, the Ministry of Agriculture, Forestry, and Fisheries reviewed the prioritization of small earth-fill dams from the viewpoint of disaster prevention, and formulated several countermeasures to safeguard such dams from heavy rain. However, due to the huge number of these hydraulic structures and the limited financial resources, it would be impossible to improve all of them. Thus, to reduce flood damage, it is desirable for local governments to establish criteria and a method to prioritize countermeasures for small earth-fill dams, based on flood damage, for maintenance management.

As a case study, the goal of this paper is to evaluate the failure risks of heavy rain and to prioritize the earth-fill dams that must be repaired and/or reinforced based on the calculated risks. The failure of the dams is examined in terms of slip failure and overflow, while the failure risks are defined as the product of failure probability and damage costs. An unsaturated seepage flow analysis, using actual rainfall conditions and the properties of small earth-fill dams, is conducted to calculate the failure probability. The damage costs are calculated based on the relationship between the results of the flood analysis after breaching and land use and asset data. Finally, an evaluation is performed to prioritize the countermeasures based on the failure risks.

METHODOLOGY

This chapter describes the methodology for calculating the failure probability of small earth-fill dams. Firstly, the types of failure modes to be adopted are simply described and the target area is shown. Secondly, hyetographs are presented; they are based on measured rainfall data and are used to calculate the failure probability. Subsequently, a flood analysis is presented; it is used in conjunction with the land use and asset data to calculate the inundation depth. The locations of acquisition of the land use and asset data are simply shown.

Failure of Dams

The failure modes of earth-fill dams due to heavy rain are usually classified as one of the three modes shown in Fig. 1 (Hori 2005). The first mode is "seepage failure caused by piping inside the dam embankment". In this mode, the fine particles leak
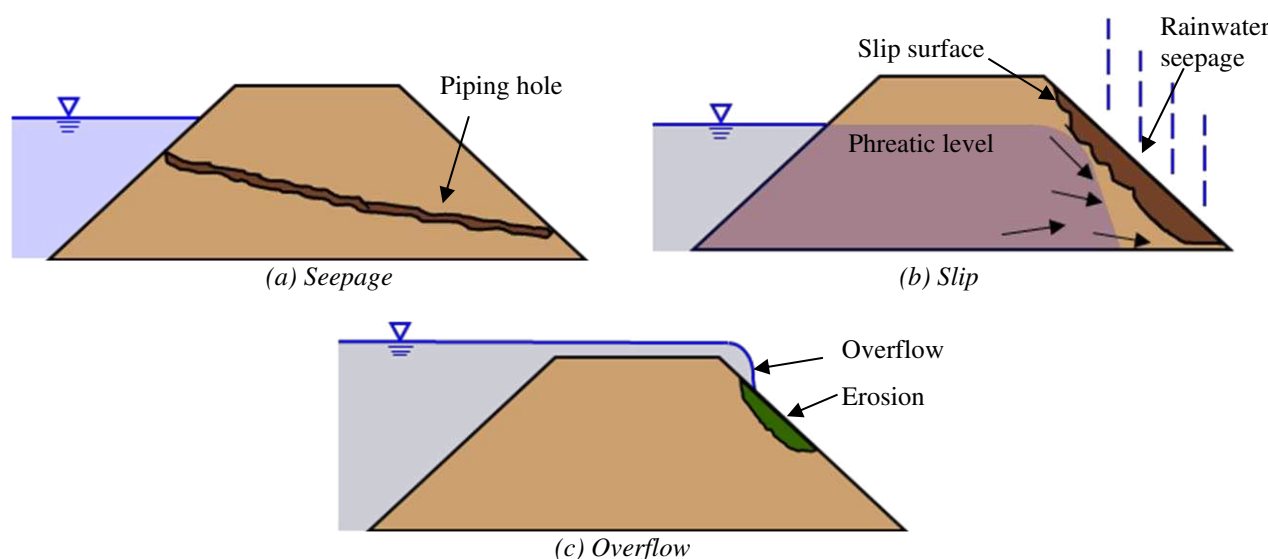

Figure 1. Failure modes of earth-fill dams in heavy rain.

out of the soil skeleton along with internal erosion, and piping holes develop. Consequently, cavities appear and the strength is reduced, ultimately causing dam failure. This mode often stems from the non-uniformity of the bank material, although it is difficult to determine its safety against seepage failure. This is because the existence of several piping holes does not necessarily cause the breaching of a dam embankment. Moreover, it is difficult to estimate the location of piping using the limited geotechnical investigation data gathered before the heavy rain, because piping is caused by soil layers with different particle size distributions and the existence of cracks. This failure mode includes backward erosion piping in small earth-fill dams, even though the failure mechanisms of internal erosion and backward erosion are different from each other. Since there is very little information on the backward erosion of small earth-fill dams brought about by the heavy rain event of July 2018 (Nishimura et al. 2018), the two types of erosion simply fall into the same failure mode.

The second mode is "slip failure of the dam embankment". This mode occurs due to the seepage of rainwater and stored water into the downstream slope of the dam embankment, raising the water level inside the dam embankment and reducing the strength of the bank material. When the shear stress exceeds the decreasing shear strength resulting from the decreasing effective stress with the increasing pore water pressure due to heavy rain in the embankment, slip failure may be produced. The third mode is "breach due to the overflow of the reservoir". When the reservoir water level rapidly increases and the capacity of the spillway becomes full, overflow is caused. The flow of stored water over the crest erodes the downstream face of the slope, dissecting the cross-section of the dam embankment.
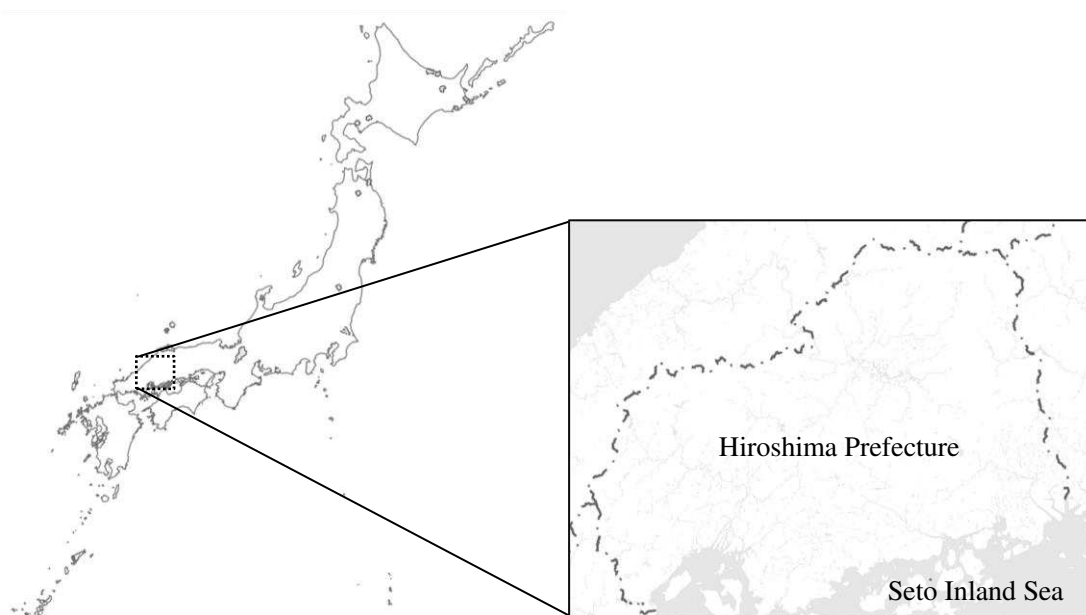

Figure 2. Location of Hiroshima Prefecture.

Table 1. Summary of earth-fill dam sites.

Dam site	Height (m)	Total volume of water (m³)	Catchment area (km²)	Spillway capacity (m³/s)	Land use of catchment area	Observatory
A	10.0	66,210	0.32	1.96	Urban district	Kure
B	9.0	155,400	0.20	2.85	Urban district	Kure
C	26.0	255,000	2.50	25.40	Forest	Shiwa
D	5.5	21,600	0.72	Unknown	Forest	Yawata
E	9.3	49,600	0.193	3.04	Forest	Tsushimi
F	6.3	13,700	0.709	0.23	Forest	Miiri
G	4.7	1,019	0.23	11.30	Forest	Hiroshima
H	9.1	6,040	0.54	11.45	Forest	Hiroshima
I	9.9	27,868	0.03	23.27	Golf course	Shiwa
J	6.5	3,100	0.01	3.00	Urban district	Kure

Case Study Area

Hiroshima Prefecture is located in the Chugoku Region of Japan along the Seto Inland Sea, as seen in Fig. 2. It has approximately 20,000 small earth-fill dams. The heavy rain event of July 2018 caused enormous damage to several of the dams in this prefecture. The 10 dams tabulated in Table 1, with different sizes and catchment areas, are employed as the target dams in this paper. Table 1 also summarizes the nearest rainfall observatory of the Japan Meteorological Agency (JMA) to each dam. The rainfall data monitored by the observatory are used to prepare a hyetograph and the flood inflow value for each dam.

Preparation of Hyetographs

The rainfall data for the target small earth-fill dams are obtained at points near the observatories, and then cumulative probability distribution curves for the maximum daily rainfall at all the observatories are plotted using past data. Three types

Table 2. Daily precipitation corresponding to return periods at each observatory.

JMA rainfall observatory	Probability distribution curve	Daily precipitation (mm/day)				
		10 years	50 years	100 years	200 years	400 years
Kure	SqrtEt	154	216	245	276	308
Shiwa	SqrtEt	161	229	260	291	325
Yawata	SqrtEt	223	320	366	414	465
Tsushimi	Gumbel	170	229	254	278	303
Miiri	Gumbel	173	227	250	273	296
Hiroshima	SqrtEt	158	219	248	278	310

(a) Kure

(b) Shiwa

(c) Yawata

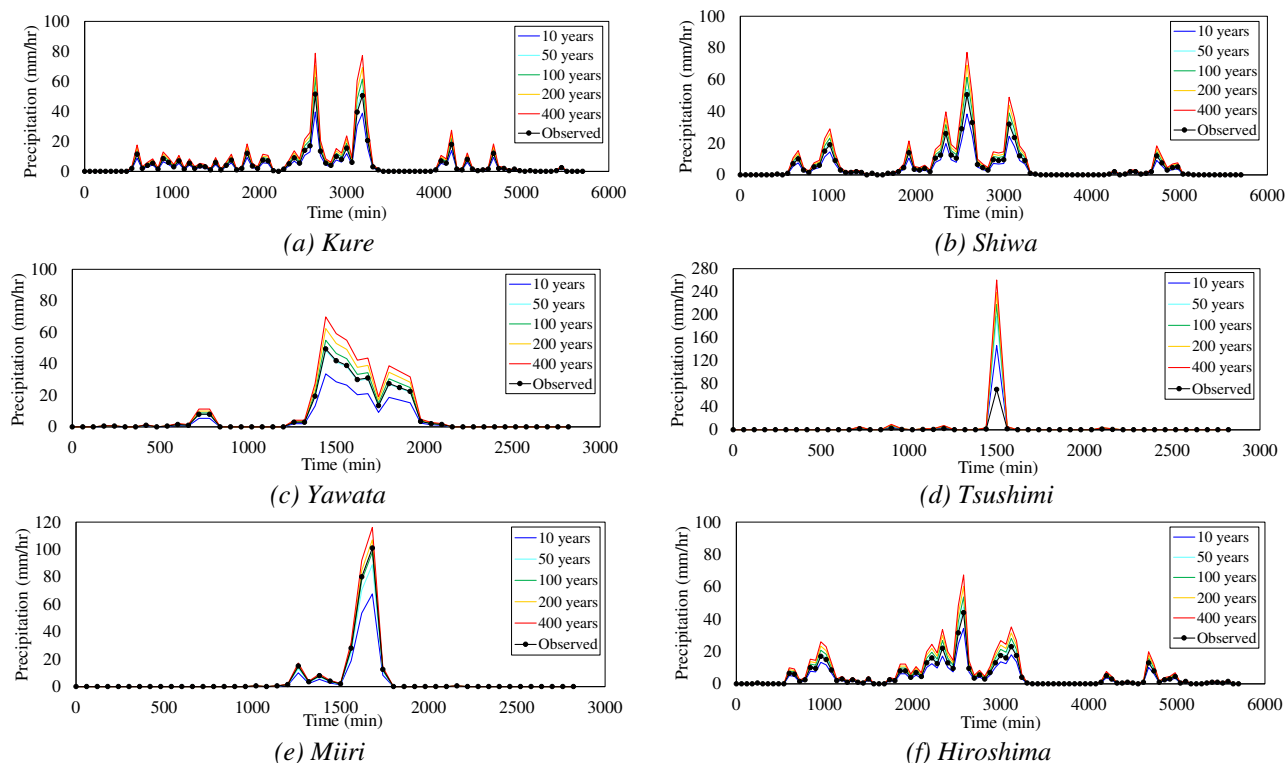*(d) Tsushimi*

(e) Miiri

(f) Hiroshima

Figure 3. Time history of precipitation at each observatory.

of distribution curves are employed: namely, the Gumbel distribution, the square root index-type maximum distribution (henceforth, SqrtEt), and the generalized extreme value distribution (henceforth, Gev), to fit the rainfall data for each site (Kuribayashi et al. 2020). Table 2 summarizes the optimal distribution curves, along which the standard least-squares criterion (abbreviated as SLSC) of distribution is smaller than 0.04 and the probability of precipitation is maximum among the three probability distribution curves. The Jackknife method is applied to effectively reduce the influence of the singular values presumed to be included in the original data set. Besides the curves, the maximum values for the daily probabilistic precipitation at each rainfall observatory are listed; they correspond to the return periods of 10, 50, 100, 200, and 400 years. The hyetograph for each return period is given by Eq. (1).

$$I_{prob}(t) = \frac{I_{probD}}{I_{obsD}} I_{obs}(t) \tag{1}$$

where $I_{prob}(t)$ is the probabilistic hyetograph, $I_{obs}(t)$ is the observed hyetograph, I_{probD} is the probabilistic daily precipitation shown in Table 2 (mm/day), and I_{obsD} is the maximum observed daily precipitation (mm/day). The observed hyetograph, which falls within the largest amount of daily precipitation during the prescribed observation period for the last five years, is employed to calculate the probabilistic hyetograph. The hyetographs, which actually include the rainfall data for the heavy rain event of July 2018 at each observatory, are presented in Figs. 3 (a)-(f).

Calculation of Failure Probability

Two types of failure that affect small earth-fill dams, namely, slip failure and overflow, are considered herein. This paper assumes that the rainfall is only a random variable. To evaluate slip failure, hyetographs are used for an unsaturated seepage flow analysis using the finite element method to indicate the rain intensity along the rainfall boundary. Changes in the reservoir water level with the time series are applied to the hydraulic head conditions in the analysis. Rainfall and the increase in the reservoir level are two of the main factors contributing to the slope instability. The computation of the water surface level is shown by the following procedure. Firstly, flood inflow Q_p (m³/s) is given by Eqs. (2) and (3):

$$Q_p = r_e \cdot A / 3.6 \tag{2}$$

$$r_e = f_p \cdot r \tag{3}$$

where r_e is the mean effective intensity within the flood concentration time, A is the catchment area (km²), f_p is the peak runoff coefficient (mm/hr), and r is the maximum rainfall intensity (mm/hr). The mean effect intensity is the average intensity of the effective rainfall. The effective rainfall is the difference between the total rainfall and the rainfall loss which is not included in the direct inflow to the reservoir due to the infiltration on the ground surface; therefore, the intensity relates to the inflow discharge. It is noted that the maximum rainfall intensity to be used is converted to the maximum daily rainfall intensity. Consequently, the phreatic levels with the time series are computed by the seepage flow analysis corresponding to the hyetographs for the five return periods, considering the increase in the water level of the reservoir and the direct effect of rainfall through the boundary conditions for the seepage analysis.

As the next stage, a circular slip calculation is performed using the modified Fellenius's method under the Mohr-Coulomb failure criterion for earth-fill dams. The slope stability analysis employed here is based on the effective stress and considers the changes in the phreatic level. The slope stability analysis determines safety factor Fs based on the unsaturated seepage flow analysis using the FEM, as follows:

$$F_S = \sum \tau_j L_j / \sum \tau_{fj} L_j \tag{4}$$

$$\tau_{fj} = c_j + (\sigma_j - u_j) \tan \phi_j \tag{5}$$

where L_j, is the length of the slip surface within the jth elements, c_j is the cohesion on the jth elements, ϕ_j is the internal friction angle on the jth elements, σ_j and τ_j are the normal stress and shear stress on the jth elements, and u_j is the pore water pressure on the jth elements. The pore water pressure is determined by the results of analyses such as that of the phreatic level. Since the stability analysis is coupled with the unsaturated seepage analysis, in which the unsteady flow analysis is conducted, the effect of the permeability on the slope stability is incorporated. The values of the parameters—such as the

strength variables for this calculation, which are deduced from field measurements and laboratory test data—are listed in Table 3. The uncertainty of the permeability is not considered, and the parameters of permeability are constant over time. Corresponding to the hyetographs for the return periods of 10, 50, 100, 200, and 400 years, the time series for the slope safety factors are calculated, and the minimum value of the safety factor in each time series is adopted as the safety factor of the corresponding return period. The failure probability for the slip failure, P_{fs}, is defined using the safety factor as follows:

$$P_{fs} = \text{Prob}\left[\max\left(\frac{1}{10}, \frac{1}{50}, \frac{1}{100}, \frac{1}{200}, \frac{1}{400}\right) \middle| F_s < 1 \right] \qquad (6)$$

The first year of the return period, for which the safety factor is smaller than 1, is adopted to calculate the failure probability, while the reciprocal of the obtained year is defined as the failure probability. For example, if the safety factors in the return period of 10 and 50 years are larger than 1 and smaller than 1, respectively, then 1/50, which is the reciprocal of the 50 years, is defined as the annual failure probability. Although the safety factors for the return periods of 100, 200, and 400 years are also smaller than 1, the failure probability, defined as the first return period in which failure occurs, is 1/50. The limit state is the condition calculated using the hyetograph from the first year of the return period, for which the safety factor is smaller than 1. Since this paper presents the safety factors for the return periods of 10, 50, 100, 200, and 400 years, the failure probability within the range of 1/400 to 1/10 is obtained. This procedure cannot provide the absolute probability of failure, but it can significantly simplify the assessment of the probability, and still has enough accuacy to evaluate the risks among the several water reservoir sites. It is noted that the rainfall directly affects the limit state—namely, there is a rise in the phreatic line due to an increase in the reservoir level—and that the direct seepage of rain into the dam embankments is strongly related to the limit state.

To evaluate the overflow type of failure, flood inflow Q_p, corresponding to the return period of each dam, is calculated using Eqs. (2) and (3). It is noted that a probability distribution curve for the maximum hourly precipitation is employed to evaluate the overflow and not the maximum rainfall intensity for the daily probability of precipitation. The failure probability for the overflow, P_{fo}, is defined by only the flood inflow and the discharge capacity of the spillway, Q_d, in Table 1 as follows:

$$P_{fo} = \text{Prob}\,[Q_d < Q_p] \qquad (7)$$

If Q_d is smaller than Q_p, the discharge capacity will be insufficient and overflow failure will occur. The failure probability is not affected by the erosion resistance to the water overflowing from the small earth-fill dam, but only determined by the amount of flood inflow and the discharge capacity for the simplification of the computation. It is emphasized that overflow failure occurs, regardless of the strength parameters, whenever Q_d is smaller than Q_p.

Table 3. Soil properties of each dam.

Dam site	Unit weight (kN/m^3)	Cohesion (kN/m^2)	Internal friction angle (degree)	Permeability (m/s)
A	20.8	35.9	17.1	8.60×10^{-6}
B	18.5	7.8	29.6	4.30×10^{-6}
C	19.8	5.1	37.1	1.99×10^{-7}
D	19.3	11.2	36.7	3.00×10^{-8}
E	19.5	8.2	38.5	1.70×10^{-7}
F	19.4	17.1	32.2	4.80×10^{-8}
G	18.9	17.3	30.7	3.30×10^{-8}
H	19.2	13.4	32.8	1.33×10^{-7}
I	17.8	11.0	32.3	9.60×10^{-6}
J	20.4	30.1	30.2	2.00×10^{-7}

Flood Analysis

Various hydrological factors, which are computed by the flood analysis, affect the magnitude of the flood damage. The maximum inundation depth of the computational results is adopted as the hydrological characteristic after the breaching. A flood analysis is carried out here by means of the shallow water equation, and the governing equations are denoted in the following forms (Toro 1999; Yoon and Kang 2004; Nishimura 2005):

$$\frac{\partial \mathbf{U}}{\partial t} + \frac{\partial \mathbf{F}}{\partial t} + \frac{\partial \mathbf{G}}{\partial t} = \mathbf{S} \tag{8}$$

$$\mathbf{U} = \begin{Bmatrix} h \\ uh \\ vh \end{Bmatrix} \tag{9}$$

$$\mathbf{F} = \begin{Bmatrix} uh \\ u^2h + gh^2/2 \\ uvh \end{Bmatrix} \tag{10}$$

$$\mathbf{G} = \begin{Bmatrix} uh \\ uvh \\ v^2h + gh^2/2 \end{Bmatrix} \tag{11}$$

$$\mathbf{S} = \begin{Bmatrix} 0 \\ ghS_{ox} \\ ghS_{oy} \end{Bmatrix} + \begin{Bmatrix} 0 \\ -ghS_{fx} \\ -ghS_{fy} \end{Bmatrix} \tag{12}$$

where t is time, u and v are the flow velocities in the x and y directions, respectively, h is the inundated water depth, and g is the gravitational acceleration. S_{ox}, S_{oy}, S_{fx}, and S_{fy} are represented as follows:

$$S_{ox} = -\frac{\partial z_b}{\partial x} \tag{13}$$

$$S_{oy} = \frac{\partial z_b}{\partial y} \tag{14}$$

$$S_{fx} = \frac{n^2 u \sqrt{u^2 + v^2}}{h^{4/3}} \tag{15}$$

$$S_{fy} = \frac{n^2 v \sqrt{u^2 + v^2}}{h^{4/3}} \tag{16}$$

where z_b is the ground elevation and n is the Manning roughness coefficient. The equations are solved by the finite volume method using the HLL-Riemann solver for indicating the flood areas of the small earth-fill dams and the distribution of the maximum inundation depth of each cell. The mesh sizes are set at 25 m and 50 m, based on GIS information collected via the Internet (Geospatial Information Authority of Japan 2020), and the minimum depth of 0.01 m and the Manning roughness coefficient of 0.035 s/m$^{1/3}$ are adopted for the analysis.

Land Use and Asset Data

The procedures for calculating the damage costs for each type of land use and asset are determined based on the Flood Control Economy Investigation Manual published by the Ministry of Land, Infrastructure, Transport, and Tourism (2005). The classifications for land use and asset data around earth-fill dam sites are acquired via the Internet (Tateishi et al. 2020). To simplify the failure risk evaluation, only free data are obtained from an online database. As for the classification of land use data—namely, paddy fields, other agricultural lands, forest, land for buildings, roads, and golf courses—the 100-m cell data on land use can be taken from the website of the National Land Information Division of National Spatial Planning and Regional Policy Bureau in the Ministry of Land, Infrastructure, Transport, and Tourism.

As for the classification of asset data—namely, the number of offices, employees, and households; the number of offices and employees classified by industry in each area; the number of households for each style of building; and the total floor area, crop acreage, and normal yield per 10 acres in the local area—are acquired from e-Stat, a portal site for Japanese Government Statistics. The normal yield per 10 acres converts to the normal yield per square meter in the calculation of the costs of agricultural damage.

The calculation method employed for each type of land use is described as follows. The land for buildings is divided into two categories: residential buildings and office buildings.

Residential building damage
= house damage + household furniture damage $\hspace{4cm}$ (17)

The damage to houses is calculated by multiplying the house assets, floor area, and damage rate as a function of the water depth estimated by the results of a flood analysis.

House damage
= house assets per area × total floor area × number of households per cell
× number of inundated cells × damage rate by inundation depth $\hspace{4cm}$ (18)

House furniture damage is defined as the product of the household furniture assets and the damage rate to the inundation depth.

House furniture damage
= value of house furniture per household × number of households per cell
× number of inundated cells × damage rate by inundation depth $\hspace{4cm}$ (19)

Office building damage consists of the following terms:

Office building damage
= redemption and inventory assets + damage of business suspension and stagnation
+ cost of emergency measures $\hspace{4cm}$ (20)

The redemption assets and the inventory assets are calculated by multiplying the number of employees by the unit price per employee. The inundation depth is obtained from the numerical results of the flood analysis.

Redemption asset damage
= depreciable assets per employee × number of employees per cell
× number of inundated cells × damage rate by inundation depth $\hspace{4cm}$ (21)

Inventory assets damage
= inventory assets per employee × number of employees per cell
× number of inundated cells × damage rate by inundation depth $\hspace{4cm}$ (22)

The damage due to business suspension and stagnation D_{ss} is expressed as follows:

Table 4. Days of business suspension and stagnation.

Inundation depth	Below floor level	Above floor level					
		Less than 0.5 m	0.5-0.99 m	1.0-1.99 m	2.0-2.99 m	Greater or equal to 3.0 m
Days of business suspension ($=n_0$)	3.0	4.4	6.3	10.3	16.8	22.6
Days of stagnation ($=n_1$)	6.0	8.8	12.6	20.6	33.6	45.2

Table 5. Relationship between inundation depth and expenditure burden of alternative activities.

Inundation depth	Below floor level	Above floor level					
		Less than 0.5 m	0.5-0.99 m	1.0-1.99 m	2.0-2.99 m	Greater or equal to 3.0 m
Unit cost (Thousands of JPY)	470	925	1,714	3,726	6,556	6,619

$$D_{ss} = M \times \left(n_0 + \frac{n_1}{2} \right) \times p \tag{23}$$

where M is the number of employees, which equals the product of the number of inundated cells and the number of employees per cell; n_0 is the number of days of business suspension; n_1 is the number of days of stagnation; and p is the additional value divided by the number of persons and days. Table 4 provides the relationship between the inundation depth and the days of business suspension and stagnation. The recovery cost is represented by Eq. (24):

Cost of emergency measures
= alternative activity expenditure burden in office sector by inundation depth
× number of offices per cell × number of inundated cells (24)

The correlation between the expenditure burden of alternative activities and the inundation depth is presented in Table 5.

Paddy field damage and soy damage are calculated as agricultural damage, because agricultural products are high in the prefecture. The inundation area is the product of the number of inundated cells and the cell area.

Paddy field damage
= normal yield per area × unit price of rice
× percentage of crop acreage of paddy field
× inundation area × damage rate by inundation depth (25)

Soy damage
= normal yield per area × unit price of rice
× percentage of crop acreage of soy
× inundation area × damage rate by inundation depth (26)

The calculation of golf course damage is based on the construction cost of a hilly course.

Golf course damage
= construction cost
× inundation area × damage rate by inundation depth (27)

This paper does not consider the land types of forests, barren land, roads, railroads, other land, rivers and lakes, beaches, and coastal zones. Other land includes building sites such as athletic stadiums, airports, racetracks, ball parks, schools, port areas, and such artificial lands. Table 6 presents the relationship between the damage rate and the inundation depth expressed by Eqs. (18)-(19), (21)-(22), and (25)-(27) (Ministry of Land, Infrastructure, Transport, and Tourism; 2005), where the inundation period of the agricultural damage is set to be 1-2 days. The damage rate of a golf course is assumed to be same as that of a plowed field. It is noted that this paper does not include the loss of life due to floods. This is mainly because only one person perished due to the breaches of small earth-fill dams in the heavy rain event of July 2018, although many people drowned due to the heavy rain (Nishimura et al. 2020).

Table 6. Relationship between damage rate and inundation depth.

Damage	Below floor Level	Above floor level					Sedimentation (Above floor level)	
		Less than 0.5 m	0.5-0.99 m	1.0-1.99 m	2.0-2.99 m	Greater or equal to 3.0 m	Less than 0.5 m	Greater or equal to 3.0 m
House	0.050	0.144	0.205	0.382	0.681	0.888	0.430	0.785
House furniture	0.021	0.145	0.326	0.508	0.928	0.991	0.500	0.845
Redemption assets	0.099	0.232	0.453	0.789	0.966	0.995	0.540	0.815
Inventory assets	0.056	0.128	0.267	0.586	0.897	0.982	0.480	0.780
Paddy field	0.210	0.240			0.370		0.700	
Soy	0.230	0.300			0.400		0.700	
Golf course	0.270	0.350			0.510		0.680	

RESULTS

Probability of Failure Due to Slip Failure

An example of the numerical results for Dam I, from the unsaturated seepage flow analysis, is exhibited in Fig. 4. The cross-section shows the surface and the phreatic levels. The time histories of the slope safety factor are shown in Fig. 5. This figure compares the slope safety factor in each return period, showing how the safety factor decreases as the return period increases. Moreover, the safety factor becomes the lowest after 3,000 minutes and exhibits a small peak before 5,000 minutes. Figure 6 presents the changes in the level of the water table inside the small earth-fill dam for representative times as well as the slip circle for which the minimum slope safety factor is given. The surface water level gradually rises from the downstream side
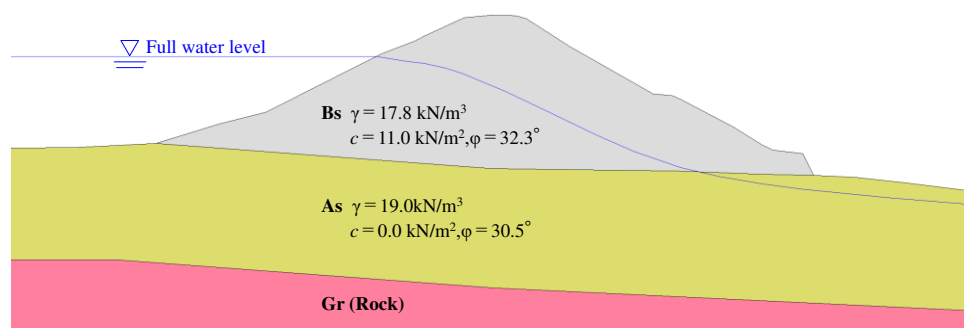

▽ Full water level

Bs $\gamma = 17.8$ kN/m^3
$c = 11.0$ kN/m^2, $\varphi = 32.3°$

As $\gamma = 19.0$ kN/m^3
$c = 0.0$ kN/m^2, $\varphi = 30.5°$

Gr (Rock)

Figure 4. Analysis cross-section (Dam I) (Kuribayashi et al. 2020).

Table 7. Minimum safety factor of each dam.

| Dam site	Hyetograph	Minimum safety factor against slip				
		10 years	50 years	100 years	200 years	400 years
A	Kure	1.819	1.807	1.807	1.807	1.807
B	Kure	1.401	1.361	1.343	1.333	1.325
C	Shiwa	1.638	1.636	1.635	1.632	1.631
D	Yawata	2.791	2.790	2.790	2.790	2.790
E	Tsushimi	1.407	1.349	1.344	1.340	1.337
F	Miiri	1.372	1.372	1.372	1.371	1.371
G	Hiroshima	1.295	1.294	1.294	1.294	1.294
H	Hiroshima	1.475	1.474	1.474	1.474	1.474
I	Shiwa	1.023	0.994	0.949	0.949	0.949
J	Kure	2.070	2.070	2.069	2.069	2.069
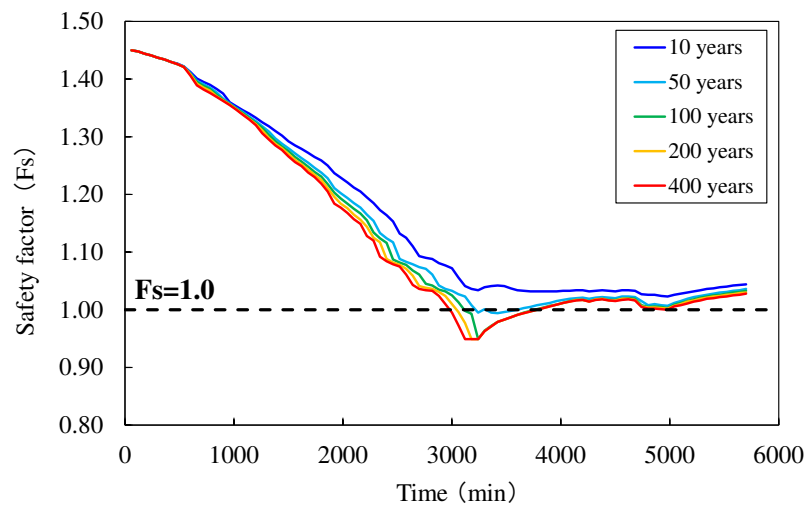
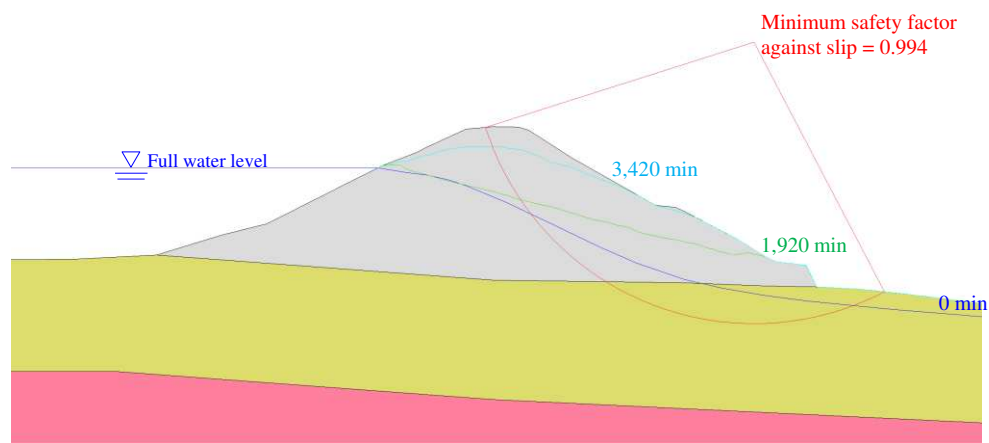*Figure 5. Time histories of slope safety factor (Dam I).*

Figure 6. Seepage water table and circular slip line (Dam I) (Kuribayashi et al. 2020).

of the dam embankment due to rainwater infiltration. The slope safety factor becomes less than 1.0 as the water table rises almost to the crest at 3,420 minutes. Table 7 shows the minimum safety factor for each return period of each small earth-fill dam. The safety factor of Dam I is lower than 1.0, whereas the safety factors of the other dams exceed 1.0 even for the rainfall of the return period of 400 years. The results for Dam I suggest that its permeability is relatively high, thus making it easier for rainwater to infiltrate. Otherwise, the shear strengths of the earth-fill and the foundation ground are relatively low.

Probability of Failure Due to Overflow

The discharge capacity of the spillway is larger than the inflow corresponding to the return period of 400 years in four of the ten dams listed in Table 8. The results indicate that overflow failure would be caused at the spillway for the remaining six dams. Figure 7 shows the correlation between the flood inflow value and the return period for the six dams. The dots indicate the return period when the flood inflow reaches the discharge capacity of the spillway. In the cases of Dams A and F, the calculated return periods are less than one year. For Dam D, it is not possible to evaluate the discharge capacity. This is because the capacity of the spillway cannot be identified and the required information is not available.

Table 8. Calculated flood inflow at each dam.

Dam site	Discharge capacity (m^3/s)	Q_p (m^3/s)				
		10 years	50 years	100 years	200 years	400 years
A	1.96	3.73	4.89	5.38	5.87	6.36
B	2.85	2.33	3.05	3.36	3.67	3.97
C	25.40	27.90	34.20	36.61	38.79	40.85
D	-	8.83	11.17	12.16	13.13	14.12
E	3.04	2.62	3.66	4.14	4.62	5.10
F	0.23	8.89	12.04	13.37	14.67	15.92
G	11.30	2.77	3.64	4.01	4.37	4.74
H	11.45	6.50	8.55	9.42	10.27	11.14
I	23.27	0.32	0.40	0.43	0.45	0.48
J	3.00	0.12	0.15	0.17	0.18	0.20

Table 9. Failure probability at each dam.

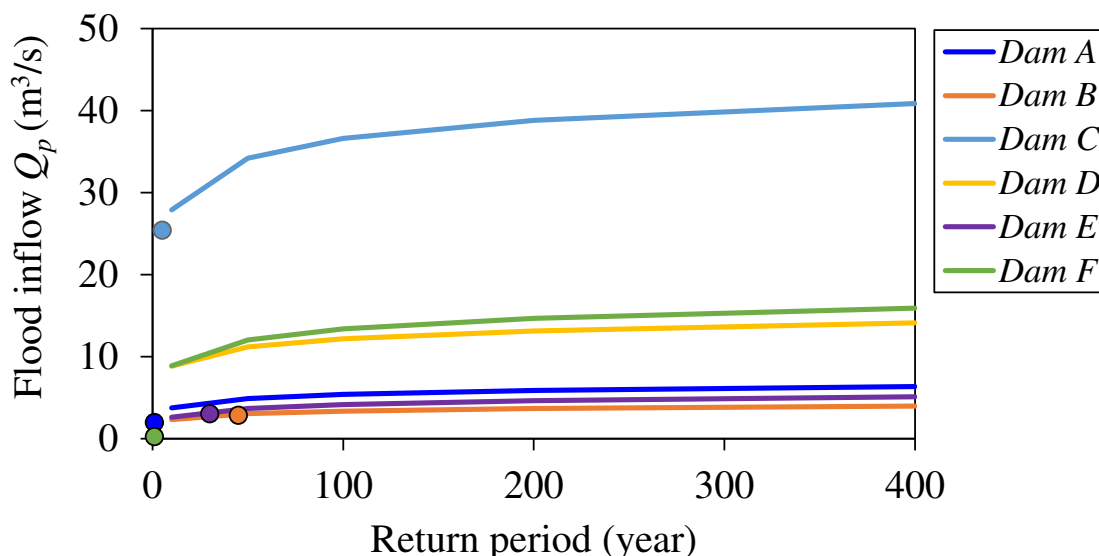| Dam site	Hyetograph	Failure probability	
		Slip	Overflow
A	Kure	1/400	1/1
B	Kure	1/400	1/45
C	Shiwa	1/400	1/5
D	Yawata	1/400	1/1
E	Tsushimi	1/400	1/30
F	Miiri	1/400	1/1
G	Hiroshima	1/400	1/400
H	Hiroshima	1/400	1/400
I	Shiwa	1/50	1/400
J	Kure	1/400	1/400

*Figure 7. Correlation between flood inflow and return period.*

Summary of Failure Probability for Each Dam

Table 9 shows the failure probability for both slip failure and overflow. For only one of the ten dams, namely, Dam I, the failure probability due to slip failure is determined by the slip failure method. The failure probability of Dam I due to slip failure means that damage may occur with the precipitation corresponding to a return period of 50 years. As the safety factors of the remaining nine dams are larger than 1.0 in each return period, the failure probability for these dams is assumed to be 1/400. For Dams A, B, C, D, E, and F, the failure probability due to overflow is determined. This paper describes the damage property of 1/1 for overflow. The overflow mode is simply defined as $Q_d < Q_p$. In fact, the overflow does not occur and the state of $Q_d < Q_p$ does not cause overflow within a very short term. This is because the water reservoirs have storage ability. Additionally, the actual inflow into the reservoir, Q_p, comes with a delay as the surface flow from the upstream area and the actual peak of the Q_p value is averaged. Consequently, the proposed approach is based on an assumption made significantly on the safety side; thus, the probability of 1/1 sometimes appears.

These results suggest that overflow, rather than slip failure, is the more dominant predisposing factor for damage to small earth-fill dams. The probability of failure due to overflow, calculated by the return period corresponding to the flood inflow, is the same as that of the discharge capacity of the spillway, falling in the range of 1/400 to 1/10. For the remaining four dams, namely, Dams G, H, I, and J, it is predicted that they will not experience damage, even due to precipitation, corresponding to the return period of 400 years.

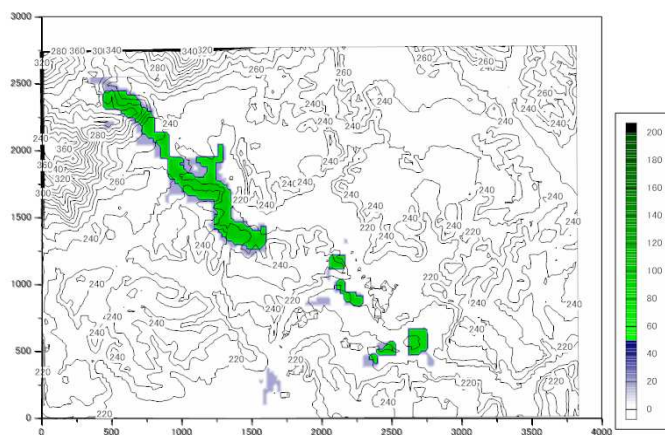**Results of Damage Costs and Failure Risks**

Figure 8 (a), (b), and (c) shows examples of the distributions of the maximum inundation depth, the damage costs to industry, and the damage costs to agriculture around Dam C, respectively. Since the land use types differ in each area, the distributions of the damage costs also differ, as illustrated in Fig. 8 (b) and (c). Moreover, the figure shows that the damage costs to agriculture are much lower than those to industry. Table 10 lists the failure risks and ranking of each earth-fill dam site. The failure risk is equal to the failure probability multiplied by the damage costs due to flooding after breaches. Employing the rankings in Table 10, local governments will be able to adequately manage the maintenance of small earth-fill dams considering the land use conditions around the target dam site under rainfall conditions.
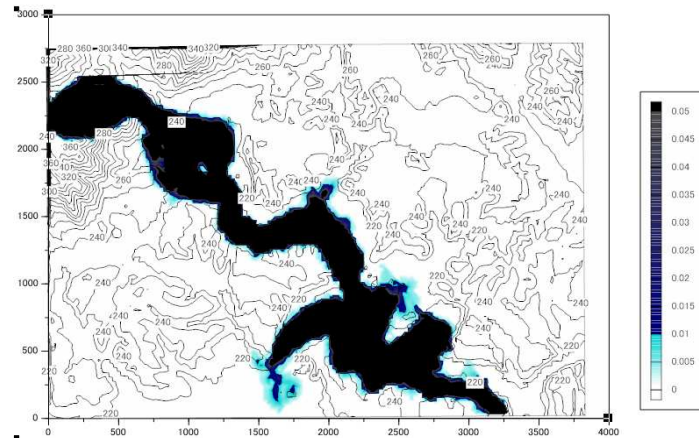
(a) Maximum flood depth (m).
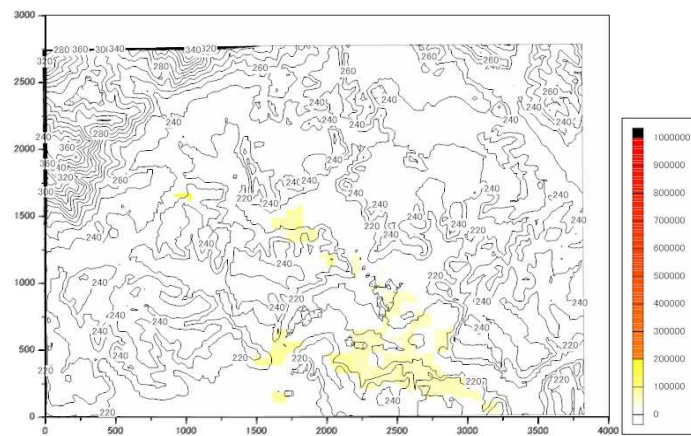
(b) Distribution of damage costs to industry (1,000 JPY/m²).

(c) Distribution of damage costs to agriculture (1,000 JPY/m²).

Figure 8. Example of distributions around Dam C.

Table 10. Results of risk evaluation.

Dam site	Probability of failure	Damage cost (Millions of JPY)	Failure risk (Millions of JPY)	Ranking
A	1/1	11,670	11,670	1
B	1/45	18,642	414	4
C	1/5	18,495	3,699	2
D	1/1	3,476	3,476	3
E	1/30	10	0.34	9
F	1/1	338	338	5
G	1/400	9,233	23	8
H	1/400	54,457	136	6
I	1/50	16	0.31	10
J	1/400	22,890	57	7

CONCLUSION

This paper has presented an evaluation of the failure risks due to heavy rain for determining the priority of countermeasures for ten targeted small earth-fill dams. To calculate the failure probability of these earth-fill dams for slip failure analysis, an unsaturated seepage flow analysis was conducted using actual measured rainfall data. The probabilities of slip failure and overflow were determined by the slip failure method and the ratio of the flood inflow to the discharge capacity of the spillway, respectively. In addition, a 2D flood analysis was carried out to obtain the inundation depth around the targeted dam sites. The damage costs were determined from the relationship between the inundation depth after breaching and the land use and asset data taken from the Internet. The failure risk was calculated as the product of the failure probability and the damage costs, and then the prioritization of the countermeasures was performed based on a comparison of the failure risk rankings.

The failure probability due to slip failure was 1/50 for only one of the ten dams, Dam I, while the failure probability for the remaining nine dams was 1/400. The damage probabilities due to overflow for all the dams were larger than or equal to those due to slip failure, except for Dam I. The damage probabilities for slip failure and overflow indicated that overflow plays a primary role in the occurrence of dam failure. Mohri (2018) reported that the number of breaches due to overflow is greater than that of slip failure in Japan; therefore, the results and the previous damage cases show a similar tendency.

The failure risks were calculated according to the presented procedure, and the ranking of each earth-fill dam site was shown by the associated risks. The prioritization of the countermeasures against floods was easily performed according to the rankings of the risks. This way, local governments will be able to adequately determine the priority of safeguarding measures for small earth-fill dams.

The approach presented here does not include model errors in the assessment of the damage costs, calculation method of the failure probability, and soil parameters. Although these additional uncertainties will contribute to the failure probability, the proposed procedure can still work well for determining the priority of the countermeasures as a practical approach to assessing the risks.

REFERENCES

Alfieri, L., Dottori, F., Betts, R., Salamon, P., and Feyen, L. (2018). "Multi-model projections of river flood risk in Europe under global warming." *Climate*, 6(1), 2018.

Geospatial Information Authority of Japan (2020). <https://fgd.gsi.go.jp/download/menu.php> (in Japanese) (Oct. 25, 2020).

Hirabayashi, Y., Mahendran, R., Koirala, S., Konoshima, L., Yamazaki, D., Watanabe, S., Kim, H., and Kanae, S. (2013). "Global flood risk under climate change." *Nature Climate Change*, 3(9), 816–821.

Hori, T. (2005). "Damage of small earth dams for irrigation induced by heavy rainfall." *Bulletin of the National Institute for Rural Engineering*, 44, 139–247.

Jonkman, S. N., and Vrijling, J. K., (2008). "Loss of life due to floods." *Journal of Flood Risk Management*, 1(1), 43–56.

Kazama, S., Sato, A., and Kawagoe, S. (2009). "Evaluating the cost of flood damage based on changes in extreme rainfall in Japan." *Sustainability Science*, 4, 61-69.

Kuribayashi, K., Tanaya, N., Kuroda, S., Kato, T., Tateishi, T., Hirata, R., Shibata, T., and Nishimura, S. (2020) "Risk evaluation for earth-fill dams due to heavy rains - Probability of failure due to heavy rains." *The Seventh Asian-Pacific Symposium on Structural Reliability and Its Applications*.

Ministry of Land, Infrastructure, Transport and Tourism (2005). "The flood control economy investigation manual (proposed)." *River Bureau*.

Mirza, M. M. Q. (2002). "Global warming and changes in the probability of occurrence of floods in Bangladesh and implications." *Glob. Environ. Change*, 12(2), 127–138.

Mohri, Y. (2018). "Reducing disaster and maintenance based on case of small earth-fill dam damage", <https://www.jiban.or.jp/wp-content/uploads/2018/07/180725saigaiSS2_13mouri.pdf> (in Japanese) (Oct. 25, 2020).

Naess, L.O., Bang, G., Eriksen, S., and Vevatne, J. (2005). "Institutional adaptation to climate change: flood responses at the municipal level in Norway." *Glob. Environ. Change*, 15(2), 125–138.

Nishimura, S., Shuku, T., Shibata, T., and Fujisawa, K. (2005). "Reliability-based design for overflow failure of earth-fill dams due to heavy rain." *Japanese Geotechnical Journal*, 30-33.

Nishimura, S., Takeshita, Y., Nishiyama, S., Suzuki, S., Shibata, T., Shuku, T., Komatsu, M, and Kim, B. (2020). "Disaster report of 2018 July heavy rain for geo-structures and slopes in Okayama." *Soils and Foundations*, 60(1), 300-314.

Tanoue, M., Taguchi, R., Nakata, S., Watanabe, S., Fujimori, S., and Hirabayashi, Y. (2019). "Estimation of direct and indirect economic losses caused by a flood with long-lasting inundation: Application to the 2011 Thailand flood." *Water resource research*.

Tateishi, T., Hirata, R., Shibata, T., Nishimura, S., Kuribayashi, K., Tanaya, N., Kuroda, S. and Kato, T. (2020). "Risk evaluation for earth-fill dams due to heavy rains - Efficient risk evaluation by response surface method." *The Seventh Asian-Pacific Symposium on Structural Reliability and Its Applications*.

Toro, E. F. (1999). *Riemann solvers and numerical methods for fluid dynamics - A practical introduction - 2nd Edition*, Springer.

United Nations Office for Disaster Risk Reduction (2018). "Economic losses, poverty & disasters.",

<https://www.unisdr.org/files/61119_credeconomiclosses.pdf>, (Oct. 25, 2020).

Winsemius, H. C., Aerts, J. C. J. H., Beek, L. P. H. V., Bierkens, M. F. P., Bouwman, A., Jongman, B., Kwadijk, J. C. J., Ligtvoet, W., Lucas, P. L., Vuuren, D. P., and Ward, P. J. (2015). "Global drivers of future river flood risk." *Nature Climate Change*, 6(4), 381–385.

Yoon, T.H., and Kang, S. -K. (2004). "Finite volume model for two-dimensional shallow water flow on unstructured grids." *Journal of Hydraulic Engineering*, 130, 678-688.

INTERNATIONAL JOURNAL OF
GEOENGINEERING
CASE HISTORIES

*The Journal's Open Access Mission is
generously supported by the following Organizations:*

dar

Geosyntec▷
consultants

engineers | scientists | innovators

CONETEC

MUD BAY DRILLING   LANKELMA   ▽ Geotech DRILLING

ENGEO

Expect Excellence